ChemCatChem

ChemCatChem
Chemistry Europe
European Chemical Societies Publishing

RESEARCH ARTICLE OPEN ACCESS

CO_2 Sorption on PEI-Impregnated Mesoporous Silica for Direct Air Capture and Subsequent Conversion to Methanol

Tobias Beger[1] | Sofia Angeli[2] | Juliane Titus-Emse[1] | Olaf Deutschmann[2,3] | Roger Gläser[1]

[1]Institute of Chemical Technology, Universität Leipzig, Leipzig, Germany | [2]Institute of Catalysis Research and Technology, Karlsruhe Institute of Technology, Eggenstein-Leopoldshafen, Germany | [3]Institute for Chemical Technology and Polymer Chemistry, Karlsruhe Institute of Technology, Karlsruhe, Germany

Correspondence: Olaf Deutschmann (deutschmann@kit.edu) | Roger Gläser (roger.glaeser@uni-leipzig.de)

Received: 25 August 2025 | **Revised:** 19 December 2025 | **Accepted:** 22 December 2025

Keywords: CO_2 adsorption | direct air capture | kinetic model | PEI | silica

ABSTRACT

Amine-impregnated mesoporous materials are studied for CO_2 sorption at conditions of direct air capture (DAC). Mesoporous silica supports with identical specific pore volume of 0.8 cm^3 g^{-1} but varying pore width (7 – 50 nm) were impregnated with polyethyleneimine (PEI) of different molecular mass (600 – 2000 g mol^{-1}) and loading (20 – 43 wt.-%). CO_2 adsorption was evaluated under dry conditions (450 ppm CO_2) across temperatures from 30 to 70°C, distinguishing the contributions of physisorption and chemisorption. The highest uptake of 1.19 mmol g^{-1} was observed for sorbents with 30 nm pores and 33.3 wt.-% PEI loading at 50°C, balancing accessible amine density and free pore volume. A temperature-dependent shift from chemisorption to physisorption was identified, particularly in larger pores, where increased polymer mobility promotes enhanced physisorption of CO_2 via the "molecular basket" effect. Long-term cycling showed that narrow pores enhance stability by anchoring PEI through hydrogen bonding, especially for low-molecular-mass PEI. A kinetic model incorporating diffusion and surface reactions reproduces experimental trends across multiple temperatures and confirms that morphology, not intrinsic kinetics, governs CO_2 uptake. This provides mechanistic insight for designing improved sorbents for low-temperature CO_2 sorption under DAC conditions as well as catalysts for subsequent conversion to methanol.

1 | Introduction

Rapid climate change caused by global greenhouse gas (GHG) emissions poses a significant threat to human health, livelihoods, and key infrastructure [1]. International agreements on the reduction of GHG emissions include the deployment of negative emission technologies (NETs). Direct air capture (DAC) technologies have emerged as an attractive component in the portfolio of solutions aimed at reducing atmospheric CO_2 concentrations [1–3].

DAC technology currently relies on two primary approaches, distinguished by their design principle for carbon capture. Liquid DAC (L-DAC) involves two closed chemical loops: a contactor capturing CO_2 from atmospheric air using an aqueous basic solution, followed by high-temperature desorption units [4]. Solid DAC (S-DAC) utilizes solid adsorbents to capture CO_2 through a cycling process with adsorption at ambient temperature and pressure, and desorption through a temperature–vacuum swing process at medium temperatures [5].

Today, only a handful of large-scale DAC plants are operational, with a few dozen more having been commissioned in Europe, North America, Japan, and the Middle East [5]. Most of the systems currently employed worldwide are based on the S-DAC technology [5] as their typically modular design lowers capital investment costs and allows for easier scalability, manufacturing, and implementation of improvements [6, 7].

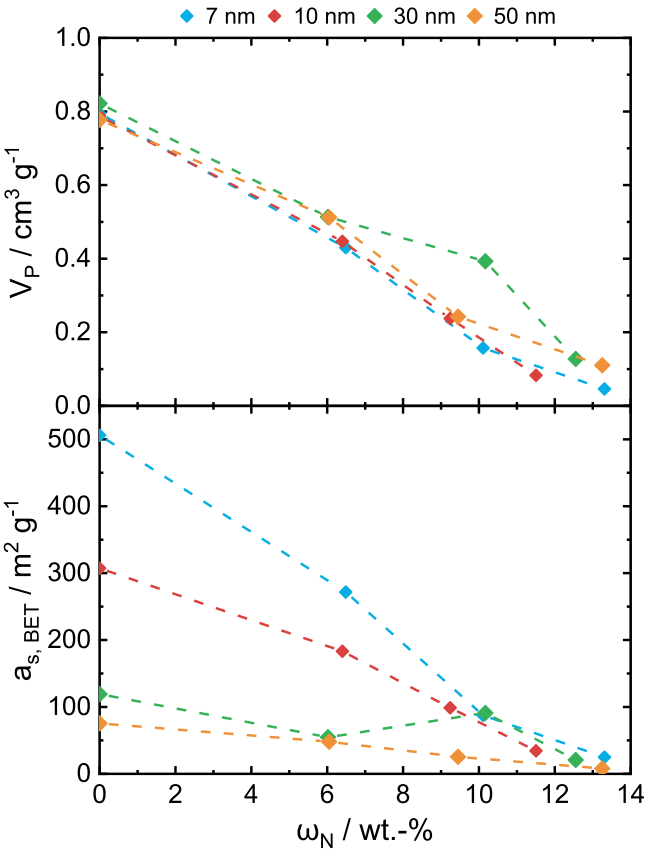

FIGURE 1 | Specific pore volume and specific surface area as a function of N content ω_N of PEI for sorbents with different support pore widths (specific pore volume for 30 and 50 nm determined by mercury intrusion porosimetry).

As one of the leading companies, Climeworks applies solid sorbent materials which are based on amines grafted onto mesoporous silica [7, 8]. These materials are well-suited for DAC due to their high uptake and selectivity in CO_2 separation with a low need for parasitic energy input, fast kinetics, multicycle stability, and tolerance toward water [9] and exhibit high CO_2 adsorption capacity and stability [10, 11]. Studies have shown that the combination of amines with porous supports increases the overall carbon dioxide uptake, revealing a synergistic enhancement that is driven by increased amine dispersion and subsequent increase in the density of accessible sorption sites [12].

Physical incorporation of amines into a porous support using impregnation methods offers an alternative approach for amine-functionalization of porous supports. This method is relatively simple and cost-effective, making it suitable for large-scale production and deployment [13]. It also allows for high amine loadings up to 19 mmol g^{-1}, which can significantly enhance CO_2 uptake capacity up to 3.50 mmol g^{-1} under dry DAC conditions [12, 14, 15].

However, high amine loadings can lead to pore blocking, reducing the accessibility and diffusion of CO_2 to the active sites and decreasing the overall efficiency of the sorbent [13]. Additionally, the physical incorporation of amines results in weaker interactions between the amines and the support material, leading to potential amine leaching during adsorption–desorption cycles [11].

Among other amines such as tetraethylenepentamine (TEPA) and tris(2-aminoethyl)amine (TREN), poly(ethylene imine) (PEI) has been investigated intensively in recent years as the prototypical aminopolymer for impregnation due to its high amine density, its facile synthesis from aziridine [16], and wide commercial availability in a large range of molecular masses. Several studies have shown that increasing PEI content progressively reduces both pore width and volume [14, 17, 18]. Consequently, larger support pore volumes have been linked to higher uptake capacities as higher amine loadings are facilitated without significantly restricting accessibility, allowing for increased dispersion of PEI within the pore system and enhancing CO_2 mass transfer [10, 11, 13, 17]. However, the specific influence of pore width remains inadequately characterized, as previous investigations have not used sorbents with constant pore volumes while systematically varying pore width dimensions.

Because of the complexity involved in the adsorption process, a typical approach for modeling the kinetics of CO_2 capture is based on fitting experimental data to established models, selecting the one that provides the best fit, and extracting information about the underlying mechanisms via parameter analysis [19–21]. The most commonly used models are pseudo-first order, pseudo-second order, Elovich- and Avrami-based models [21–24]. The pseudo-first order kinetic model is mainly used for surface diffusion-limited processes. The pseudo-second order kinetic model initially describes gas-solid adsorption controlled by the chemical interaction of CO_2 with the surface. The Elovich kinetic model assumes that the rate of adsorption decreases exponentially as the amount of adsorbate increases. The Avrami model usually presents the best fit to the experimental results, because it allows for a fractional reaction order. In addition, a double-layer model has been proposed for the sorption of "molecular basket" sorbents [25].

Current research on DAC sorbents predominantly quantifies total CO_2 uptake without differentiating between chemisorption and physisorption. This distinction, however, is crucial to a deeper understanding of the CO_2 adsorption mechanism, which has been proposed as a "molecular basket" consisting of a large pore volume material loaded with a CO_2-philic substance to cover the pore walls and space to selectively pack CO_2 in condensed form inside the pores [26, 27]. Moreover, chemisorption capacity is crucial in the context of a subsequent catalytic conversion of the captured CO_2 with renewable hydrogen to value-added products such as methanol [28]. If noble metal nanoparticles are placed in intimate proximity to the amine functionalities inside pores, a cyclic conversion of CO_2 and H_2 to methanol was shown to be possible [28].

The mechanism of chemisorption and reaction of CO_2 within amine-containing polymers is suggested to proceed similarly to aqueous amines [29]. Initially, the nucleophilic attack by the amine nitrogen on the carbon atom of CO_2 generates a zwitterionic intermediate, which subsequently undergoes either intermolecular proton transfer with another amine (Brønsted base) to form ammonium carbamate or intramolecular hydrogen transfer leading to carbamic acid, depending on adsorption condi-

tions, amine type, and water presence. Several investigations have characterized these reaction intermediates using experimental techniques such as FTIR/DRIFTS [30–32] and NMR [33–39] as well as theoretical calculations [34, 40–43], predominantly identifying ammonium carbamate and carbamic acid species [35, 44–46]. While different theoretical investigations focus on calculating the transition states and the barriers of the elementary reactions for different materials [34, 47], to the best of our knowledge, there is no lumped kinetic model reported that can globally describe the chemisorption of CO_2, decoupled from the physisorption contribution.

This study aims to investigate how the pore width of the support affects the CO_2 uptake capacity in PEI-impregnated porous silica by eliminating the influence of the pore volume. Commercial silica with pore widths across the mesopore range, maintaining the same specific pore volume, is used, and PEI loading and molecular mass are varied to gain insights into the adsorption mechanism. The loading range represents different stages of pore filling, with literature of impregnated polyamine identifying 30–70 wt.-% to achieve the highest CO_2 uptake capacities [12]. The stability of the sorbents is investigated over multiple adsorption/desorption cycles and under static temperature conditions. Due to the differentiation between chemisorption and physisorption, the experimental data are used to develop a global kinetic model to describe the chemically captured CO_2 and enable adsorbent column simulations. Such a model could serve as a basis for an in-depth investigation of physisorption models for DAC applications. Finally, the prepared materials are meant to serve as supports for Pt nanoparticles for the direct conversion of the captured CO_2 to methanol.

2 | Results and Discussion

2.1 | Sorbents

The textural properties of the commercial silica materials were verified using nitrogen sorption and mercury intrusion porosimetry. Modal pore widths were determined to be 5.8, 8.0, 30.5, and 49.5 nm, as shown in Figure S1, closely matching manufacturer specifications of 7, 10, 30, and 50 nm, respectively. Simultaneously, a key feature of the unloaded support material is the identical specific pore volume of 0.8 $cm^3\ g^{-1}$ for all pore widths, consequently leading to vastly different specific surface areas, as shown in Figure 1.

In order to validate the successful impregnation of PEI onto the mesoporous silica support material with systematic control over the loading, elemental and thermogravimetric analyses were carried out (Figure S2 in ESI). Across the targeted loading range, both analysis methods are in high agreement, confirming target and experimental loadings for 20.0 and 33.3 wt.-% PEI. Only at the highest loading of 42.9 wt.-%, a slight negative deviation from the target loading is observed.

As evidenced from the nitrogen sorption isotherms (Figure S3), the amount of adsorbed nitrogen decreases with increasing PEI content in mesoporous silica while the general shape of the hysteresis loop remains unchanged. This suggests that the pore structure and connectivity remain largely intact as the PEI is predominantly filling the pores continuously rather than causing pore blockage, which supports the interpretation of a layer-like polymer loading rather than external surface aggregation.

Specific surface area and pore volume help to identify differences in the utilization of the support pore space. As shown in Figure 1, an almost linear decrease in both $a_{s,\,BET}$ and V_P is observed for all sorbents, independent of support pore width, upon increasing PEI loading, represented by nitrogen content of the polymer. At maximum PEI loading, these values approach zero, indicating that the reduced loading efficiency can be attributed to the complete filling of the finite internal pore volume. Even higher loadings could only be achieved by polymer deposition on the external surface of the particles. However, previous studies suggest that this is detrimental for CO_2 adsorption performance, and larger PEI loadings are primarily achieved by higher specific pore volumes [48–50]. Furthermore, (localized) pore blocking may significantly impact CO_2 sorption by restricting diffusion pathways. This may result in prolonged equilibration times, which is generally undesirable for industrial applications that benefit from rapid adsorption–desorption cycles [51].

2.2 | CO_2 Adsorption

The experimental design based on particle size, pore width, PEI loading, PEI molecular mass, and adsorption temperature gives rise to a total of 108 data points for which total and chemisorption uptake were determined, as described in the experimental section. Analyzing the effects of individual parameters within this dataset presents challenges due to the interaction of factors and the issue that the experimental uncertainty often exceeds the effect of the parameter. Thus, boxplots are used to facilitate comparison of individual parameters through statistical measures such as mean value, standard deviation, and total range.

2.2.1 | Effect of Particle Size

For two particle size fractions (mean particle size of 83 and 98 µm, respectively), the total uptake q_{total} for CO_2 sorption at 30°C ranges between 0.18 and 1.11 mmol g^{-1} and 0.20 and 0.97 mmol g^{-1}, respectively (Figure 2). Considering that these values include all PEI loadings investigated, these results compare well with equally PEI-loaded porous sorbents such as SBA-15 [12, 15, 52]. It should be noted that in the comparison of the best-performing materials from the literature with the material with the highest uptake here, differences can be explained by higher amine contents and improved sorption site accessibility facilitated by higher pore volumes, improving amine efficiency. For instance, a similar PEI-loaded commercial silica with 10.5 mmol g^{-1} amine content resulted in a CO_2 uptake of 2.36 mmol g^{-1} under DAC conditions with an amine efficiency of 0.22 and a support pore volume of 1.3 $cm^3\ g^{-1}$, compared to 0.8 $cm^3\ g^{-1}$ here [53], similar results were obtained in several studies reported in the literature [50, 54–56].

No significant differences in mean or standard deviation of q_{total} and q_{chem} were found for the two particle size fractions at adsorption temperatures of 30°C, 50°C, and 70°C (Figure 2). This indicates that no internal diffusion limitations are present

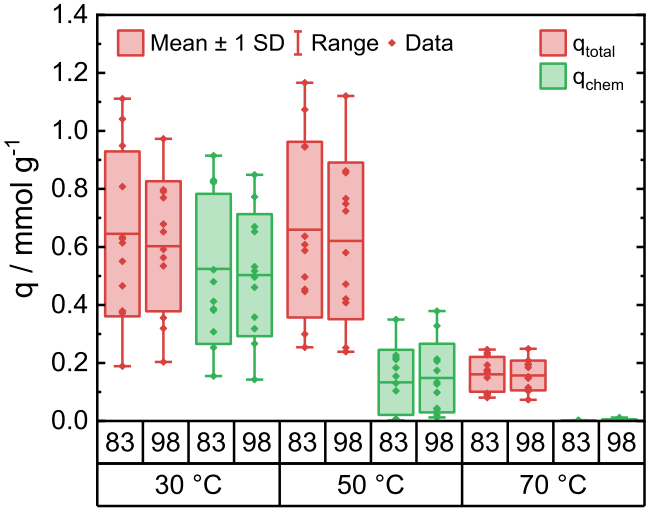

FIGURE 2 | q_{total} and q_{chem}, for two particle size fractions (mean particle size in μm) and different values of adsorption temperature (for all w_P, PEI loadings and a PEI molecular mass of 600 g mol^{-1}).

within the particle size range investigated. This could be partially attributed to the considerable overlap in particle sizes between the two fractions, with mean particle sizes of 83 ± 38 μm and 98 ± 50 μm, respectively (see Figures S4 and S5).

2.2.2 | Effect of Pore Width

Previous studies have identified the support pore volume as a key parameter for PEI-impregnated sorbents, as larger pore volume enables higher PEI loading, which increases the number of amine sites available for CO_2 adsorption [57]. The maximum amine loading was calculated to increase from 60.6% to 67.1% when the specific pore volume was increased from 1.54 to 2.04 cm^3 g^{-1} for MCF, which was reflected accordingly in the experimentally achieved amine loading and CO_2 uptake [58].

Besides the number of adsorption sites, sufficient unoccupied pore space is crucial for CO_2 diffusion and interaction with amine groups. Less unoccupied pore space was found to increase mass transfer resistance and lower the CO_2 capture efficiency [14, 58].

As shown in Figure 3, the highest values for q_{total} and q_{chem} are observed for a pore width of 30 nm at 30°C adsorption temperature (0.85 mmol g^{-1} and 0.71 mmol g^{-1}, respectively). Across all pore widths, chemisorption dominates the adsorption with a share of 79% – 87% of q_{total}, generally higher for larger pores. At 50°C, q_{total} remains the highest at 30 nm with a value of 0.91 mmol g^{-1} while q_{chem} decreases significantly and remains almost unchanged for all pore widths, representing only a share of 28% of q_{total}, now decreasing with increasing pore width. At 70°C, chemisorption is no longer detected, though a residual q_{total} of about 0.15 mmol g^{-1} is retained on all sorbents.

The effect of pore width here can be best explained by assuming a direct interaction of PEI molecules with the pore walls in their immediate vicinity. At 30°C, the polymer is assumed to exhibit a bulk-like behavior, with adsorption predominantly governed by chemisorption occurring at the polymer surface. In small pores, the polymer chains are strongly confined, likely adopting flattened conformations in contact with the silica walls. This spatial restriction promotes a high local density of accessible amine groups, favoring strong chemisorption through the formation of carbamate or carbamic acid. Conversely, in larger pores, PEI chains are much less constrained and can adopt a more coiled, three-dimensional configuration within the pore volume. These structural features facilitate the creation of inter-chain voids, which support the formation of physisorption via weaker van der Waals forces and induced dipole interactions.

When the adsorption temperature is increased to 50°C, PEI viscosity is lowered, allowing for a higher polymer chain mobility and swelling toward the pore center [59]. These conformational changes effectively generate new free cavities for the accommodation of additional CO_2. This behavior has previously been described as the "molecular basket" effect, where the CO_2 is selectively packed in a condensed form inside the pores, facilitated by a CO_2-philic pore surface [27].

In large pores, this leads to a net increase in uptake, despite the thermodynamic disadvantage for chemisorption at higher temperatures. It is quantitatively reflected in the temperature-dependent changes in uptake for different pore widths. Between 30 and 50 °C q_{total} decreases by up to 10% in 7 nm pores but increases by up to 16% in 50 nm pores (Figure S6a).

Simultaneously, chemisorption decreases by 68% – 78% as expected for the higher temperature. This demonstrates that the shift in adsorption mode from chemisorption to physisorption effectively compensates for the decline of chemisorption capacity.

2.2.3 | Effect of PEI Loading

Similarly, the highest value of q_{total} is observed at a PEI loading of 33.3 wt.-% for both 30°C and 50°C with a value of 0.83 mmol g^{-1} (Figure 3 right). Similarly, Chaikittisilp et al. [60] found a CO_2 sorption capacity of 1.05 mmol g^{-1} for SBA-15 (pore width: 7 nm) loaded with 39.9 wt.-% PEI. Sorbents with 20 wt.-% PEI exhibits a lower uptake, which can be attributed to the lower number of amine adsorption sites. Conversely, sorbents with 42.9 wt.-% PEI shows lower uptake, likely due to polymer crowding and restricted diffusion. The effect of PEI loading parallels that of pore width, as increasing the adsorption temperature to 50°C alters the adsorption mechanism: q_{total} decreases by 10% for sorbents with 20.0 wt.-% PEI loading, increases marginally by 1% for 33.3 wt.-%, and increases significantly by 20% for sorbents with 42.9 wt.-% PEI loading (see Figure S6b). While q_{chem} generally decreases with increasing temperatures, the absolute share of chemisorption positively correlates with PEI loading (Figure 4).

It is assumed that at low PEI loadings, the polymer forms a thin layer coating the pore walls offering a high specific amine accessibility and substantial free pore space for CO_2 sorption. This results in higher shares of physisorption while preventing thermal polymer swelling. This could provide additional physisorption capacity to compensate for reduced chemisorption at elevated temperatures. At intermediate PEI loadings, bulk domains of the polymer start to form as a loose interior polymer network inside the pores. This reduces the available free volume for physisorp-

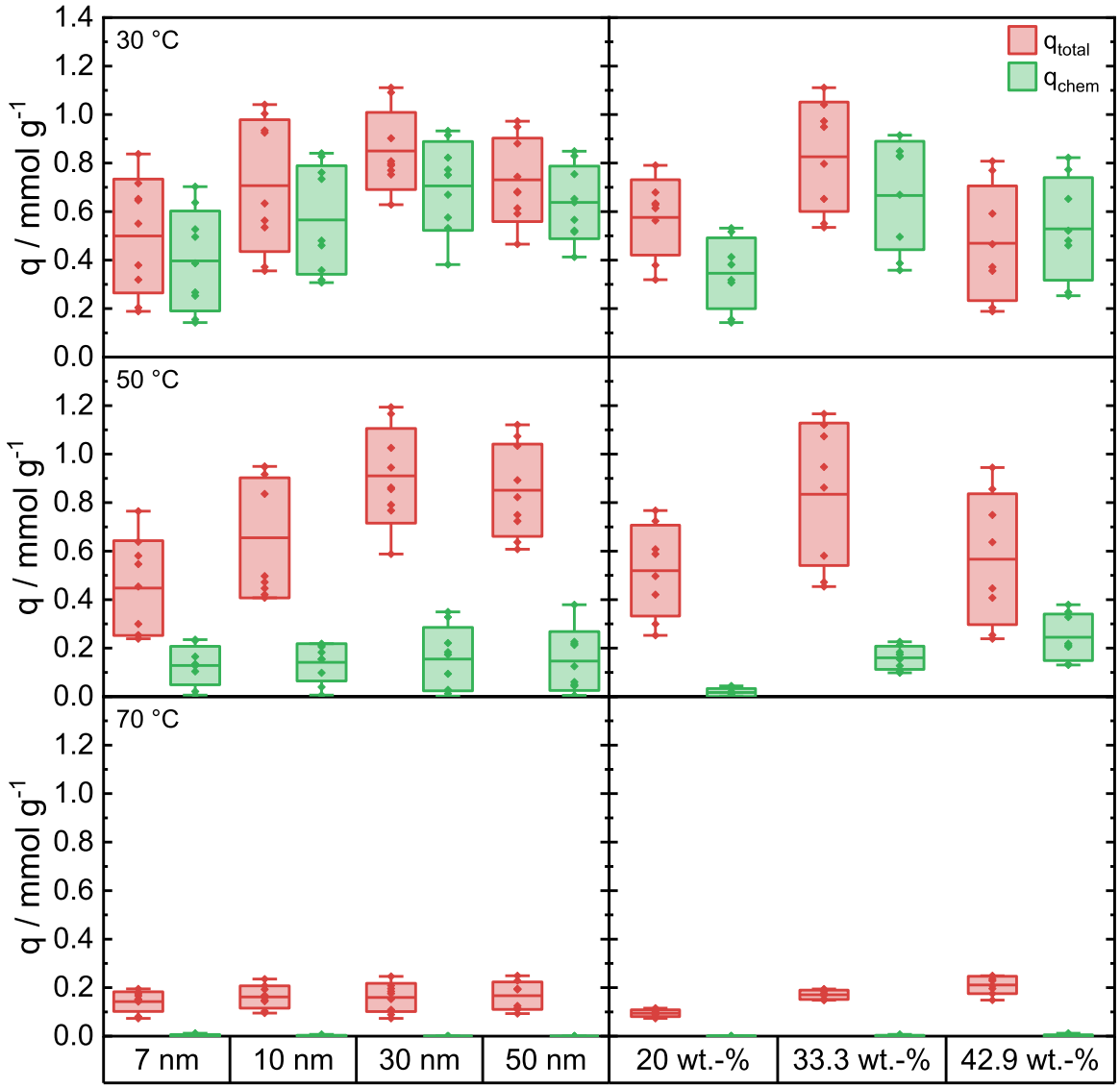

FIGURE 3 | q_{total} and q_{chem}, for different pore width (left), PEI loading (right), and adsorption temperature.

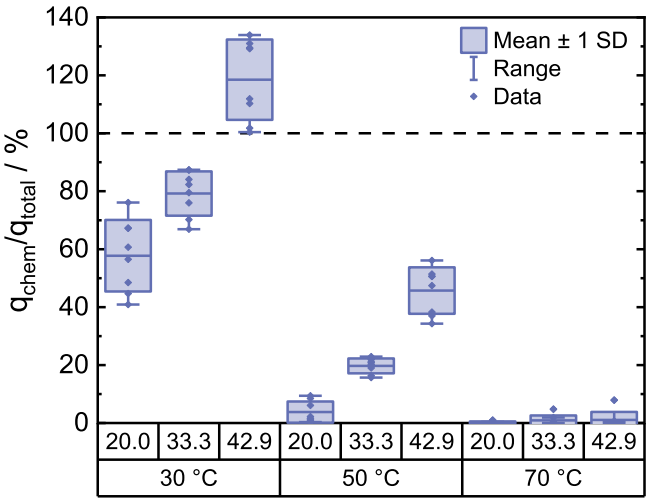

FIGURE 4 | Fraction of chemisorbed on total CO_2 uptake for different adsorption temperatures and PEI loading (in wt.-%).

tion and thus shifts the adsorption mode toward chemisorption. However, these domains permit thermal swelling, allowing new cavities to form. These cavities accommodate physisorbed CO_2 and compensate for the lower share of chemisorption at higher temperatures.

At the highest PEI loading, where, based on nitrogen sorption/mercury intrusion porosimetry 85.8% to 92.2% of the pore is filled with PEI, the increased number of amine sites does not directly translate into higher chemisorption, as many sorption sites become concealed inside the polymer bulk and therefore sterically inaccessible at 30°C. In addition, the lack of residual free space hinders physisorption. Upon increasing the temperature to 50°C, enhanced polymer mobility makes the concealed amine groups accessible, leading to a significant increase in chemisorption with increased PEI loading rising from 0.02 to 0.24 mmol g^{-1} between 20 and 43 wt.-% [61]. Furthermore, a portion of the chemisorption sites transition into physisorption sites at higher temperatures [62], a behavior that remains observable even at 70°C.

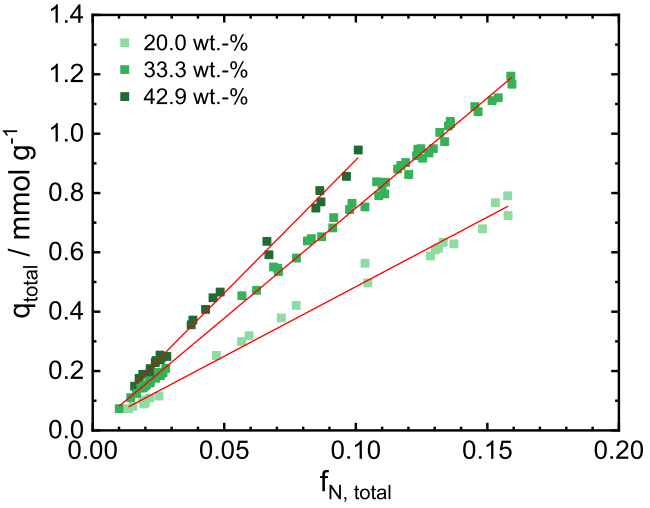

FIGURE 5 | Total CO_2 uptake as a function of amine efficiency for different values of PEI loading.

As shown in Figures 5 and S6, each PEI loading corresponds to a distinct linear regime with a characteristic slope for both q_{total} and q_{chem} representing the PEI loading-dependent amine accessibility. Sorbents with lower PEI loading exhibit higher amine accessibility, enabling them to achieve identical CO_2 uptakes at higher amine efficiency compared to higher-loaded sorbents. As an example, a sorbent with 20 wt.-% PEI loading achieved a q_{total} of 0.76 mmol g^{-1} at $f_N = 0.153$, while a sorbent with 43 wt.-% PEI loading with a similar q_{total} is at $f_N = 0.087$. However, given that in dry conditions two amine groups are necessary to capture one CO_2 molecule, limiting amine efficiency to a maximum of 0.5 [63], higher loading values could ultimately lead to more uptake, provided that sufficient accessibility would be maintained.

Based on these findings, it can be concluded that a sorbent with a support pore width of 30 nm and a PEI loading of 33.3 wt.-% provides the highest CO_2 uptake.

2.2.4 | Effect of PEI Molecular Mass

Further insight into the interaction between aminopolymer and pore walls and width can be obtained by examining PEI of varying molecular mass, as this, for example, has an effect on the PEI viscosity. As CO_2 sorption was highest for 33.3 wt.-% PEI loading, the following studies for varying PEI molecular mass were conducted at 33.3 wt.-% loading. A lower molecular mass consistently results in higher CO_2 uptakes (Figure 6). This aligns with literature attributing this observation to the higher viscosity and the higher proportion of amines that are active for CO_2 capture [18, 64].

Branched PEI comprises primary (1°), secondary (2°), and tertiary (3°) amine groups, each exhibiting distinct CO_2 adsorption characteristics. Primary amines preferentially bond with CO_2 through the formation of intermolecular ammonium carbamates, while secondary amines predominantly stabilize CO_2 as carbamic acid [46]. Tertiary amines, conversely, capture CO_2 solely as alkylammonium bicarbonate in the presence of water [65]. Hence, under the applied conditions, no significant contribution of tertiary amines to q_{chem} is expected.

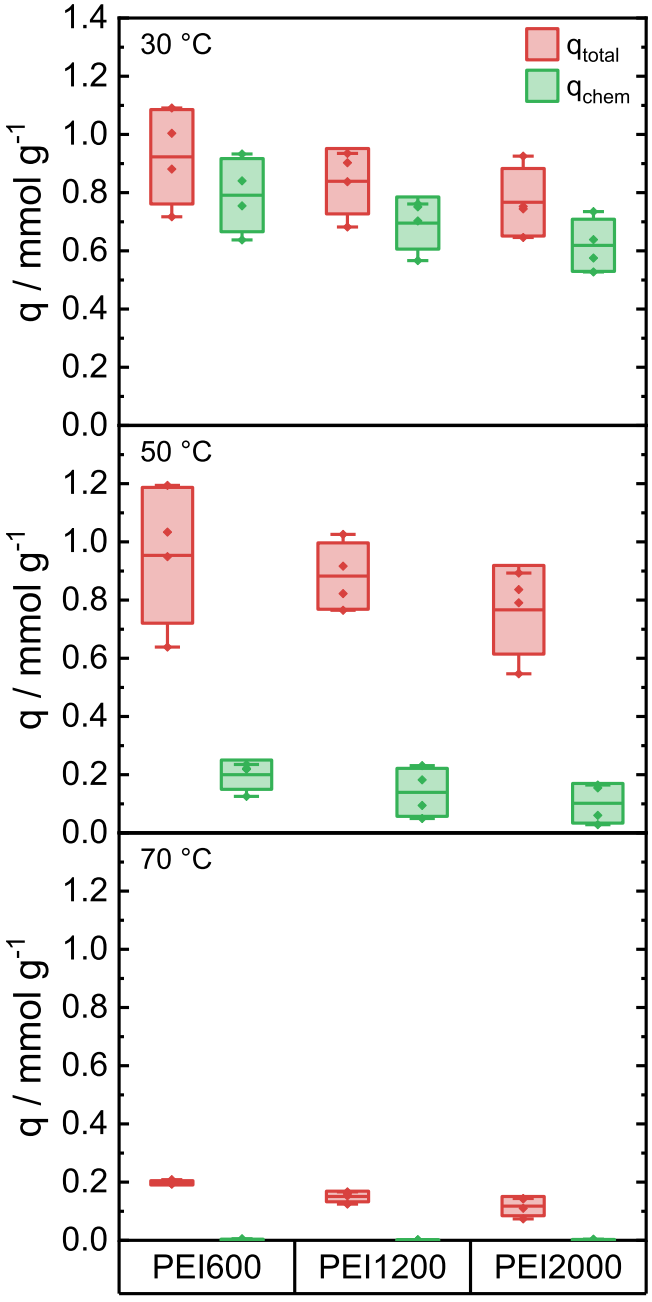

FIGURE 6 | q_{total} and q_{chem}, at different temperatures for sorbents loaded with PEI of different molecular mass.

The relative proportions of these amine types can be quantified using ^{13}C NMR spectroscopy (Figure S9) [66–68]. While the expected composition of PEI synthesized using the acid-catalyzed polymerization from aziridine is 1°:2°:3° = 1:2:1, it was demonstrated that commercially available PEI deviates from this ratio and tends to converge to 1:1:1 at M_w = 1,000,000 g mol^{-1} [16, 69]. Here, analysis of PEI composition reveals a consistent trend: as molecular mass increases from 600 to 2000 g mol^{-1}, the share of primary amines decreases while the share of tertiary amines grows (see Figure S8). Specifically, 1°:2°:3° amine ratios shift from 1:0.9:0.6 for PEI600 to 1:1:0.7 for PEI1200 to 1:1:0.8 for PEI2000.

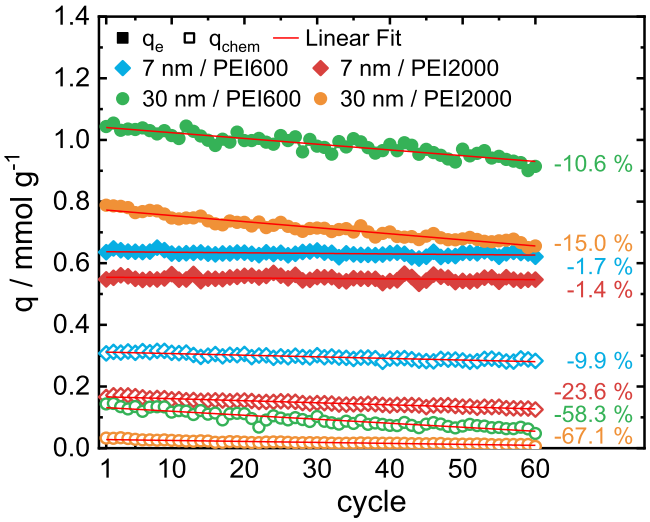

FIGURE 7 | q_{total} and q_{chem} of sorbents with different pore width and molecular mass of PEI with a loading of 33.3 wt.-% over 60 adsorption/desorption cycles.

As shown in Figure S10a, amine efficiency decreases with increasing molecular mass of PEI (f_N = 0.09 for PEI600, 0.08 for PEI1200, and 0.07 for PEI2000). If the differences in amine type distribution were solely responsible for the observed differences in uptake, equal values for f_N would be expected after normalization for potential sorption sites. However, as shown in Figure S10b, while higher values are produced, the negative correlation persists (f_N = 0.12 for PEI600, 0.11 for PEI1200, and 0.10 for PEI2000), indicating that the difference of 4.3% in potential sorption sites is insufficient to fully account for the variation in CO_2 uptake. Likely, the interaction between PEI and the pore walls needs to be considered as the polymer chains interact with the support surface, especially through the amine groups of PEI with silanol groups of the silica surface. This might also result in improved stability of the impregnated PEI. Consequently, not all amine groups are effectively available for CO_2 adsorption.

2.3 | Sorbent Stability

2.3.1 | Cycle Stability

The stability of sorbents with different PEI molecular mass was evaluated over 14 adsorption/desorption cycles (Figures S11 and S12), where no major differences were observed, with the average loss in q_{total} being −3.4% for PEI600, −4.3% for PEI1200, and −2.7% for PEI2000.

Extended cycling experiments over 60 cycles were performed to identify long-term interaction effects of pore width and PEI molecular mass on uptake stability that may only be revealed at a high number of cycles. The selected sorbents are characterized by small and large pores (7 and 30 nm), and small and large PEI molecular mass (600 and 2000 g mol^{-1}), as shown in Figure 7.

Initially, uptakes match previous results, with the supports with the larger pores (w_P = 30 nm) having higher q_{total} (1.04 and 0.79 mmol g^{-1}) while for smaller pores (w_P = 7 nm) lower q_{total} (0.63 and 0.54 mmol g^{-1}) results. However, due to a higher fraction of chemisorption, higher q_{chem} were observed (0.31 and 0.16 mmol g^{-1}, compared to 0.14 and 0.03 mmol g^{-1} for 30 nm).

Over 60 cycles, all sorbents loose CO_2 uptake, but the extent depends considerably on their pore width and PEI molecular mass (Figure 7). For the materials with 7 nm pores, PEI600 retains a q_{total} of 0.62 mmol g^{-1} and a q_{chem} of 0.28 mmol g^{-1}, corresponding to a fitted linear loss of only −1.7% in q_{total} and −9.9% in q_{chem}. Similarly, PEI2000 results in a q_{total} of 0.55 mmol g^{-1} and a q_{chem} of 0.13 mmol g^{-1}, with a linear loss of −1.4% in q_{total} and a more pronounced −23.6% decline in q_{chem}. By comparison, sorbents with the larger 30 nm pores lose more uptake capacity with PEI600 showing a q_{total} of 0.91 mmol g^{-1} and a q_{chem} of only 0.048 mmol g−1 after 60 cycles, corresponding to a linear loss of −10.6% and −58.3%, respectively. PEI2000 dropped even further to a q_{total} of 0.66 mmol g^{-1} and a q_{chem} of just 0.006 mmol g^{-1}, associated with a −15.0% loss in q_{total} and −67.1% in q_{chem}.

Studies in the literature typically report drastically fewer regeneration cycles, with performance on silica supports ranging from stable up to 7.8% decrease in CO_2 uptake after 20 cycles, mostly at a desorption temperature of 110°C [12]. PEI-loaded halloysite nanotubes achieved a loss in uptake of 3.28% after 50 cycles using a regeneration temperature of 80°C [70]. To explain the uptake loss under cyclic operation, two potential pathways of loss of active sites are considered: polymer leaching involves the detachment and ejection of polymer chains out of the support pores, while polymer degradation involves the chemical damage of the polymer chain or cleavage of amine groups due to thermal or CO_2-induced stress, for example, oxidative chain scission or carbamate-induced backbone cleavage.

This mechanism was investigated by determining the elemental composition of sorbents after the regeneration cycles at 100°C. Additionally, to isolate the thermal effect, a treatment at 100°C was performed, eliminating CO_2 adsorption/desorption steps while maintaining the total thermal exposure.

A measurable loss of nitrogen was observed across all samples, primarily influenced by pore width. For the sorbents with 7 nm pores, nitrogen content in simulated regeneration materials decreased by −3.75% (PEI600) and −4.72% (PEI2000); for the sorbents with 30 nm pores, the losses were −12.48% and −11.98%, respectively. These results are comparable with the cycled materials, confirming the simulation as a valid proxy (see Figure S13). Considering the carbon content, an increase of +5.8% for 7 nm pores with PEI600, and stability or a slight decrease for the other materials is observed. The divergence between nitrogen and carbon behavior supports the idea that the polymer backbone remains largely intact, while it undergoes chemical alteration and amine groups are selectively cleaved, indicating a combination of amine leaching and chemical degradation, rather than full-chain leaching.

This highlights the stabilizing influence of confinement in small pores. In the 7 nm pores, spatial constraints enforce close contact between PEI and the silica surface, promoting dense hydrogen bonding between amine groups and surface silanol (Si–OH) groups. This interaction stabilizes the PEI in the smaller pores to resist large-scale rearrangement or polymer loss. In contrast,

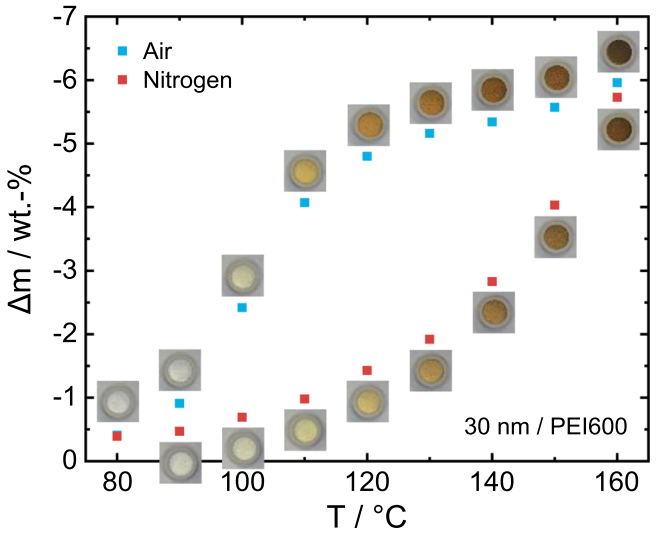

FIGURE 8 | Mass loss and visual change of sorbents with 20.0 wt.-% PEI loading after treatment at the specified temperature for 12 h in different atmospheres.

the larger 30 nm pores allow for more relaxed polymer conformations, reducing the density and strength of these hydrogen bonds. Although the polymer remains within the pores, its looser configuration facilitates local chain rearrangements and makes it more susceptible to amine degradation or detachment. This behavior results in the stronger loss of CO_2 uptake over 60 cycles for the sorbents with larger pores, as shown in Figure 7.

The strength and density of hydrogen bonds are governed by the basicity and steric accessibility of the amines involved. Primary and secondary amines, more prevalent in lower molecular mass PEI, interact more strongly with silanol groups; sorbents with PEI of lower molecular mass exhibit improved stability. This parallels findings from amine–alcohol complexation studies, where linearity of the N–H···O bond and lack of steric obstruction enhance hydrogen bond stability [71].

2.3.2 | Thermal Stability

To further evaluate the thermal degradation of PEI, thermogravimetric analyses in different atmospheres were performed. The degree of decomposition of PEI can be estimated by a combination of mass loss and change in color of the materials (Figure 8). Initially, no difference between atmospheric conditions can be observed with a mass loss of 0.4 wt.-% and no color change at 80°C. At higher temperatures, ambient atmosphere results in a stronger decomposition with a sharp increase in mass loss between 90 and 110°C, rising from −0.9 wt.-% to −4.1 wt.-%. After this, decomposition continues at a lower rate up to a mass loss of −6.0 wt.-% at 160°C. For comparison, in an inert nitrogen atmosphere, a more gradual decomposition starting above 90°C is observed, roughly matching the other material at 160°C with a mass loss of −5.7 wt.-%.

The color of the sorbents changes starting from 100°C with a yellow-orange-brown progression that consistently appears darker for air-treated sorbents at the same treatment temperature. The degradation behavior can be attributed to different decomposition mechanisms, considering physical degradation such as evaporation and leaching of amines and chemical degradation through oxidation [72]. Under inert conditions, degradation is largely thermally driven, and PEI decomposes primarily through random scission of C–N and C–C bonds. The subsequent mass loss is caused by the evaporation of the formed gaseous amines and can be reduced by increasing the molecular mass of PEI [73].

Secondary amines have been identified more prone to oxidative degradation [74–77] but can be stabilized by hydrogen bonding [78, 79]. In-situ DRIFT spectroscopy has been used to show that oxidative degradation of PEI in air leads to the formation of carbonyl- and imine-containing species, such as amides, imines, and possibly carboxylic acids. Stronger characteristic bands as a measure for the degree of oxidative degradation were detected when treatment temperature or duration was increased [72]. In combination with the findings from CO_2 sorption and in agreement with the literature, it can be concluded that the regeneration temperature for the sorbents should be lowered to a temperature between 80°C and 100°C [73]. This would improve sorbent stability while CO_2 desorption from active sites is completed at lower regeneration temperatures.

2.4 | Adsorption Kinetics

2.4.1 | Impact of Morphology and Sorption Conditions

While adsorption temperature has been identified as one of the strongest predictors for uptake capacity, it also significantly affects apparent adsorption kinetics, as it is affecting all subprocesses involved in CO_2 capture, including chemisorption, diffusion, and physisorption (see Figure S14). Apparent adsorption half-time, $t_{0.5}$, is defined as the time required to reach half of the equilibrium uptake and provides information on the overall kinetics. At 30°C and 50°C, adsorption half-times were nearly identical at 8.1 and 8.3 min, respectively; however, increasing the temperature to 70°C significantly reduced $t_{0.5}$ to 3.3 min. After normalization for uptake capacity, the values across all temperatures converged, indicating that the smaller $t_{0.5}$ observed at 70°C primarily reflects the lower equilibrium uptake rather than inherently faster sorption.

The influence of temperature is further evident in the time to reach the maximum adsorption rate, $t_{r_{max}}$, which decreased not only in value but also in standard deviation with increased adsorption temperature: 2.0 ± 1.2 min (30°C), 1.3 ± 0.42 min (50°C), and 0.82 ± 0.06 min (70°C). This indicates that at lower temperatures, apparent adsorption kinetics are governed by a wider range of factors related to the structural and morphological properties affecting the internal diffusion, while at higher temperatures, reaction kinetics become more dominant, and CO_2 desorption is favored. The maximum adsorption rate, r_{max}, remained constant at 0.055 mmol g^{-1} min^{-1} for 30 and 50°C but dropped by 22% to 0.043 mmol g^{-1} min^{-1} at 70°C.

Pore width plays a moderate but systematic role in apparent adsorption kinetics (see Figure S15). Sorbents with larger pores

show slightly longer absolute adsorption half-times, owing to their higher total adsorption capacities, while shorter normalized half-times are caused by higher internal diffusion rates. This is also demonstrated by higher maximum adsorption rates in larger pores, where reduced mass transfer resistance facilitates faster gas transport to internal active sites.

PEI loading also has an impact on adsorption kinetics as higher loadings increase diffusion resistance in the pore system, but at the same time, the amount of available active sites is increased (see Figure S16). Adsorption half-times were almost doubled between 20.0 and 42.9 wt.-% PEI, increasing linearly from 4.5 to 8.23 min. Normalized adsorption half-times remain similar for both 20.0 and 33.3 wt.-% at 13.7 min g $mmol^{-1}$ but increase significantly to 24.6 min g $mmol^{-1}$ for 42.9 wt.-%. This is an indication that, beyond a certain threshold, residual free pore volume becomes so limited that the internal diffusion limitation affects the overall performance significantly. Likewise, the maximum adsorption rate is decreased by 13% for the highest loading compared to similar values for the lower loadings investigated. At the same time, $t_{r_{max}}$ shifts to earlier times from 1.56 min for 20.0 wt.-% to 1.11 min for 42.9 wt.-%. Since the highest adsorption rate occurs almost immediately upon CO_2 exposure, severe diffusion limitations lead to CO_2 reacting predominantly with the most accessible surface amines, resulting in a sharp initial uptake spike that cannot be sustained due to the slower internal diffusion.

In contrast, within the investigated range, PEI molecular mass (Figure S17) exhibits only a minor influence on apparent adsorption kinetics, primarily due to differences in viscosity and the share of tertiary amines hindering molecular movement of the polymer chains and therefore access to reactive amine groups.

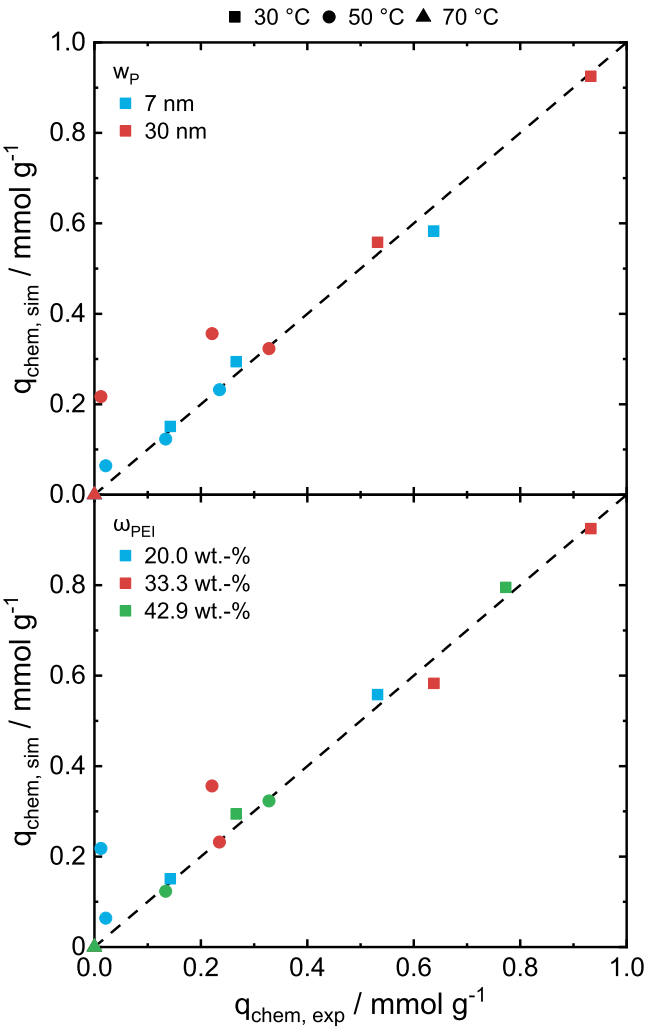

FIGURE 9 | Parity plot of experimental data and model-based predictions of q_{chem} at different PEI loading and pore width.

2.4.2 | Chemisorption Kinetics and Internal Diffusion Simulations

The overall capture performance of the materials is controlled by an interplay of chemisorption kinetics and pore diffusion limitations resulting from the pore structure of the materials. Additionally, the physisorption contribution can drastically affect the overall capture performance as a result of the pore structure, by enabling sorption mechanisms such as the "molecular basket" mechanism.

In order to decouple the underlying processes, the CO_2 captured via chemisorption uptake is modeled by developing a lumped kinetic model coupled with a simple pore diffusion model. The aim is to establish a basic kinetic model for CO_2 capture simulations which, when coupled with different physisorption models, would enable a more in-depth investigation into the "molecular basket" mechanism.

The lumped chemisorption reaction mechanism is composed of a second-order adsorption reaction of CO_2 and its desorption. In addition to the reaction of the surface with CO_2, the diffusion within the pores was modeled based on the individual properties of the materials, such as pore width and pore volume (particle porosity), and the predictions were subsequently fine-tuned by adjusting the tortuosity of the materials. Tortuosity can be considered to be non-uniform among the materials due to the three-dimensional structure of PEI-loaded pores [80].

The above models were solved together with a transient fixed-bed reactor model to predict q_{chem} for a representative selection of the materials presented above. Driven by the experimental parametric investigation in this work, the simulation results are summarized in a parity plot in Figure 9 with regard to adsorption temperature, PEI loading, and pore width.

The model predictions capture the chemisorption performance well by reflecting the temperature trend of decreasing q_{chem} between 30°C and 50°C and showing no chemisorbed CO_2 at 70°C due to the domination of the desorption under these conditions. The kinetic parameters for the investigated temperatures are shown in Table S1. The values of the kinetic coefficients reported in literature are strictly related to the kinetic model used and the assumptions within (e.g., pseudo-first order, Avrami, etc.) and also span a wide range of values depending on the conditions [19–21, 81]. In the model described in this work, CO_2 chemisorption is considered via two surface reactions (adsorption and desorption), and the rate is expressed as a surface rate, which renders a direct comparison of the values unfeasible.

However, the ratio of the forward and the reverse reaction rate constant, that is, the equilibrium constant, becomes equal to unity at 87°C in agreement with the literature for PEI-impregnated materials [82].

For the model predictions, the pore width and pore volume were included in the calculation of the effectiveness factor that describes how much the chemisorption rate is limited by diffusion. Additionally, the availability of the active amine sites in each sample is considered via the specific surface area of the sample and the N content as measured by the elemental analysis described above. This led to a unique set of model input parameters for each sample, even though the chemisorption reaction kinetic coefficients were kept constant for all samples.

In Figure 9, the majority of the symbols lie along the parity line, indicating that the differences in CO_2 capture among the materials are not caused by the kinetics of the chemisorption, but rather that the materials' pore structure actually defines the chemisorbed CO_2 uptake. The largest deviation from the experimental measurements is observed for materials with 30 nm pores at an adsorption temperature of 50°C. As outlined above, it is believed that the lower viscosity of PEI at this temperature leads to an increased polymer chain mobility. In the case of large pores, this affects the dispersion of PEI on the pore walls, causing it to concentrate more into the pore center rather than covering the pore walls evenly [26]. The model simulations reported in Figure 9 consider that each sample is characterized by its unique properties, while also assuming these properties remain constant across varying conditions, resulting in the deviation between the simulation result and experimental value. The outliers refer to PEI loadings of 20 and 33.3 wt.-%, while in the case of 42.9 wt.-% PEI loading, pore blocking caused by PEI likely led to much lower pore width and hindered the effect of the viscosity. A systematic investigation into the effect of the operating conditions on the PEI distribution into the pores would provide valuable insight and enable refinement of the model.

The largest deviation from the experimental measurements is observed for materials with 30 nm pores at an adsorption temperature of 50°C. As outlined above, it is believed that the lower viscosity of PEI at this temperature leads to an increased polymer chain mobility. In the case of large pores, this affects the dispersion of PEI on the pore walls, causing it to concentrate more in the pore center rather than covering the pore walls evenly [26]. The model simulations reported in Figure 9 consider that each sample is characterized by its unique properties, while also assuming these properties remain constant across varying conditions, resulting in the deviation between the simulation result and experimental value. The outliers refer to PEI loadings of 20 and 33.3 wt.-%, while in the case of 42.9 wt.-% PEI loading, pore blocking caused by PEI likely led to much lower pore width and hindered the effect of the viscosity. A systematic investigation into the effect of the operating conditions on the PEI distribution into the pores would provide valuable insight and enable refinement of the model.

As this model is capable of decouple and accurately describe chemisorption kinetics and diffusion processes, the physisorption contribution of the "molecular basket" warrants a dedicated in-depth investigation and modeling due to the complexity of the mechanism. This step is especially relevant under the low-temperature conditions typical of DAC applications, where physisorption effects may significantly influence overall CO_2 uptake performance.

3 | Conclusions

This study shows that the pore width of mesoporous silica as supports for poly(ethylene imine) has a significant impact on CO_2 sorption under conditions of DAC.

Across all pore widths (7 – 50 nm), chemisorption dominates CO_2 uptake at 30°C, particularly in smaller pores. As temperature increases, a transition occurs in which physisorption becomes increasingly relevant, especially in larger pores, due to enhanced polymer chain mobility and swelling. The formation of voids between the polymer chains supports physisorption via weak, non-specific interactions, characteristic of the "molecular basket" effect. The highest total CO_2 uptake of 1.19 mmol g^{-1} is achieved for sorbents with 30 nm pores and 33.3 wt.-% PEI loading, offering a balance between available and accessible amines, adequate polymer chain mobility, and sufficient free pore space for diffusion and temperature-enhanced physisorption.

Confinement of PEI in the mesopores also plays a dominant role in preserving CO_2 uptake over repeated adsorption–desorption cycles. Sorbents with a small support pore width of 7 nm exhibit lower initial capacities but show markedly reduced degradation over 60 ad-/desorption cycles, attributed to stronger interaction of polymer chains with the silica pore walls.

Differentiation between experimentally quantified physisorbed and chemisorbed CO_2 emphasized the necessity to understand the underlying individual steps. To this end, a lumped kinetic model was developed to describe the chemisorption coupled with an internal diffusion model. Simulation results accurately predict chemisorption uptake using a single set of kinetic parameters. The uptake by chemisorption is primarily governed by the pore morphology of the sorbent support, which affects both the uptake rate and the accessibility of amine sites. Further studies will focus on a detailed investigation into the effect of the operating conditions on the impregnated poly(ethylene imine) and the resulting pore structure in order to further refine the current model. Furthermore, a systematic study and modeling of the physisorption mechanisms occurring within the temperature range of DAC applications, combined with the existing chemisorption and diffusion model, would significantly advance the understanding of the overall adsorption process. Such efforts are essential for optimizing both material design and operational parameters for application in DAC of CO_2.

Eventually, the PEI-impregnated mesoporous silica materials will be utilized as supports for Pt nanoparticles. Thus, the CO_2 capture function will be combined with a catalytic functionality to provide the cooperative interaction needed for directly converting the chemisorbed CO_2 with hydrogen from renewable sources to methanol. Thus, not only CO_2 sorption and storage, but a subsequent utilization of the captured CO_2 for carbon capture and utilization (CCU) under dynamic conditions is enabled.

4 | Experimental Section

4.1 | Materials

Chromatorex MB70 75/200, MB100 75/200, MB300 75/200, and MB500 75/200 were purchased from Fuji Silysia. Branched polyethylene imine (PEI600, M_w = 600 g mol^{-1}, 99% / PEI1200, M_w = 1200 g mol^{-1}, 99% / PEI2000, M_w = 2000 g mol^{-1}) was obtained from thermoscientific. Methanol (MeOH, 100%) was purchased from VWR. All chemicals and reagents were of analytical grade and were used as received.

4.2 | Sorbent Preparation

Commercial spherical mesoporous silica (Chromatorex) with reported particle sizes 75 – 200 µm and pore widths of 7, 10, 30, and 50 nm has been wet impregnated with PEI with loadings of 20.0 wt.-%, 33.3 wt.-% and 42.9 wt.-%. Materials were fractionated using fine sieves into two groups (< 100 µm and > 100 µm). The wet impregnation procedure was adapted from the literature [26] with slight modifications. The target amount of PEI ($M_n \approx$ 600, 1200, 2000 g mol^{-1}) was dissolved in 8 g (10.1 mL) of methanol in a 25 mL round-bottom flask, 1.0 g of silica was added, and the mixture was stirred for 30 min. Then, the solvent was removed under reduced pressure, and the remaining solid was dried at 80°C at 4 mbar overnight.

4.3 | Sorbent Characterization

4.3.1 | Nitrogen Sorption

Textural properties were characterized by means of nitrogen sorption with a Microtrac BELSORP MINI X. Specific pore volume, pore width distribution, and specific surface area were determined from the isotherms. The samples were activated at 150°C for at least 48 h, after which the adsorption and desorption isotherms of nitrogen were recorded at −196°C. Specific surface area was determined from the adsorption branch using the BET method [83], and pore width distribution was determined from the desorption branch using the BJH method [84].

4.3.2 | Mercury Intrusion Porosimetry

Materials with pore widths of 30 and 50 nm were additionally characterized by means of mercury intrusion porosimetry using a ThermoScientific PASCAL 140. Measurement parameters were set to a contact angle of 140°, a surface tension of 0.48 N m$^{-1,}$ and a maximum pressure of 400 MPa. Intrusion data were utilized to calculate specific pore volume and pore width distribution using Washburn's equation [85].

4.3.3 | Elemental Analysis

Elemental analyses were carried out using a vario MACRO cube by Elementar Analysensysteme GmbH to determine C, H, and N content. Approximately 20 mg of sample together with 80 mg of tungsten trioxide were folded into a 2 × 2 cm piece of Sn foil and combusted at 1200°C, creating a temperature up to 1800°C inside the Sn foil, after which gaseous incineration products were reduced over a copper catalyst. Selective column trapping and release was used to guarantee baseline separation of N_2, CO_2, H_2O, and $SO_{2,}$ which were quantified using a thermal conductivity detector.

4.3.4 | Thermogravimetric Analysis

Thermogravimetric analyses were conducted on a Hitachi STA300 instrument. For each analysis, approximately 10 mg sample was placed inside a 60 µl alumina crucible and heated at a rate of 10°C min^{-1} up to 800°C in air to determine PEI loading, or with a rate of 5°C min^{-1} up to temperatures between 80 and 160°C in air or nitrogen atmosphere and held for 12 h to investigate thermal stability of sorbents.

4.3.5 | Particle Size Analysis

Particle size distribution of supports was determined using a CILAS 1064L particle size analyzer and the software Size Expert. Before the measurement, the sample container was flushed with water for about 2 min, and a background measurement was carried out. Afterwards, a sufficient amount of sample was added to achieve an obscuration between 3 and 10, and then measured in the flow cell using dynamic light scattering with a laser.

4.3.6 | Nuclear Magnetic Resonance Spectroscopy

Nuclear magnetic resonance spectroscopy (NMR) experiments were performed using an AVANCE III HD 400 NMR spectrometer by Bruker with a 2-channel-BBFO probe with an ATM unit and a 16-position sample changer at a frequency of 400 MHz. For the measurement, about 100 mg of PEI was transferred to a quartz tube and dissolved in around 0.4 mL of D_2O.

4.3.7 | CO_2 Adsorption

For CO_2 uptake measurements, 25 mg of sorbent was placed between two layers of glass wool inside a glass tube with a diameter of 10 mm enclosed by a heater. Gas flow was controlled via mass flow controllers to maintain a total flow of 0.1 L min^{-1} and the effluent CO_2 concentration was measured using a Hartmann&Braun URAS 10E NDIR gas analyzer. Samples were activated under He flow at 100°C for 120 min, then each sorption cycle consisted of an adsorption step under 450 ppm CO_2 in He flow at 30 – 70°C for 120 min, a purge step under He flow at the same temperature for 45 min, and a desorption step under He flow at 100°C for 30 min. CO_2 adsorption capacity was calculated using Equation (1) for the adsorption branch (total uptake, q_{total}) and Equation (2) for the desorption branch (chemisorption uptake, q_{chem}), based on Chatterjee and Schiewer [86].

$$q_t = \frac{p \cdot \dot{V}_{tot} \cdot c_0 \cdot \int_0^t \left(1 - \frac{c}{c_0}\right) dt}{R \cdot T \cdot m} \quad (1)$$

$$q_t = \frac{p \cdot \dot{V}_{tot} \cdot \int_0^t (c)\, dt}{R \cdot T \cdot m} \quad (2)$$

p—pressure, $\dot{V}_{tot}$—total gas flow rate, c_0—inlet CO_2 concentration, c—outlet CO_2 concentration, R—universal gas constant, T—temperature, m—sorbent mass.

Amine efficiency was calculated as the uptake capacity at the stationary state (considered to be (pseudo-)equilibrium) from CO_2 breakthrough experiments divided by the nitrogen content from elemental analysis.

4.4 | Kinetic Model and Adsorption Simulations

4.4.1 | Reactor Model

Adsorption simulations were carried out using the DETCHEM^{PBR_TRANSIENT} simulation package. This is a 1D fixed-bed reactor model, resembling the sorption column employed, which assumes no radial variations in flow properties as well as negligible axial diffusion compared to the convective terms [87]. The governing equations include the continuity Equation (3) and the gas phase species balances Equation (4):

$$\frac{d(\rho u)}{dz} = a_v \sum_{i \in S_g} M_i \dot{s}_i \tag{3}$$

$$\rho u \frac{dY_i}{dz} + Y_i a_v \sum_{i \in S_g} M_i \dot{s}_i = M_i \left(a_v \dot{s}_i + \dot{\omega}_i \varepsilon \right) \tag{4}$$

ρ – fluid phase density, z – axial coordinate of the reactor, u – superficial velocity, a_v – total particle surface area to catalytic bed volume ratio, $\dot{s}_i$ – surface phase reaction rate, M_i – molar mass of species i, Y_i—mass fraction of gas phase species i, $\dot{\omega}_i$—gas phase reaction rate, ε—catalytic bed porosity.

As CO_2 must diffuse into the pores of the material, it encounters adsorption sites, leading to a concentration gradient. In cases where the diffusion rate is lower than the adsorption rate, diffusion becomes the rate-limiting step. The pore diffusion was modeled using an effectiveness factor, which is the ratio of the surface reaction rate under diffusion limitations to the surface rate in the absence of diffusion limitations (for spherical particles).

$$\eta_i = \frac{\overline{\dot{s}_i}}{\dot{s}_i} = \frac{3}{\varphi^2} \{\varphi [\coth \varphi] - 1\} \tag{5}$$

$$\varphi = L \sqrt{\frac{k}{D_{eff,i}}} \tag{6}$$

φ—Thiele modulus, $D_{eff,i}$—mixed diffusion coefficient, k—reaction rate coefficient.

The mixed diffusion coefficient is calculated from contributions from both molecular and Knudsen diffusion:

$$D_{eff,\,i} = \frac{\epsilon_p}{\tau} \overline{D_i} \tag{7}$$

$$\overline{D_i} = \frac{1}{D_{mol,\,i}} + \frac{1}{D_{knud,\,i}} \tag{8}$$

ϵ_p—particle porosity, τ—tortuosity, $D_{mol,\,i}$—molecular diffusion coefficient, $D_{knud,\,i}$—Knudsen diffusion coefficient.

External mass transfer resistances to the observed reaction rate under the experimental conditions were assessed using the Mears criterion [88] and were excluded, no external mass transport model was considered in the simulations.

4.5 | Chemical Model

The surface reaction rate $\dot{s}_i$ of the surface species i is described as

$$\dot{s}_i = k_{f,k} \prod_{i=1}^{N_g+N_s} c_j^{\upsilon'_{ik}} - k_{r,k} \prod_{i=1}^{N_g+N_s} c_j^{\upsilon''_{ik}} \tag{9}$$

where the rate coefficients follow an Arrhenius-type expression:

$$k_k = A_k T^{\beta_k} \exp\left[-\frac{E_{a,k}}{RT}\right] \cdot \prod_{i=1}^{N_s} \theta_i^{\mu_{ik}} \tag{10}$$

k_k—rate coefficient in the step k for the given reaction, $E_{a,k}$—activation energy, A_k—pre-exponential factor, β—fitting parameter regarding the temperature dependency of the reaction rate, θ_i—surface coverage, μ_{ik}– model parameter to modify the reaction order for species i, here considered $\mu_{CO_2 k} = 2$.

Even though CO_2 does not dissociate during adsorption on amines, prior studies have shown that the reaction barrier is significantly lowered in the presence of two amine molecules, as one amine acts as a nucleophile to attract CO_2, while the other functions as a Brønsted base to facilitate proton exchange [45, 46, 89]. The lumped kinetic model developed in this work considers a global, reversible surface reaction of gaseous CO_2 with the amine sites, here denoted as "s," toward adsorbed CO_2.

$$CO_2\,(g) + s \rightleftharpoons CO_2\,(ads)$$

The number of available active sites was estimated based on the nitrogen content and the specific surface area of each material.

$$\Gamma = \frac{\frac{\omega_N}{100}\frac{m}{A_N}}{a_{s,\,BET}} \tag{11}$$

Γ—surface site density, ω_N—nitrogen content (from elemental analysis), m—sample mass, A_N—atomic mass of nitrogen, $a_{s,\,BET}$—specific surface area.

The reaction coefficients of the forward and the backward reaction are given in Table S1. It should be noted that the lumped parameters should be treated as a set of parameters, rather than individual parameters describing only adsorption or desorption processes.

Acknowledgments

The authors acknowledge support of this work by the Deutsche Forschungsgemeinschaft (DFG), the German Research Foundation, within the priority program SPP 2080 "Catalysts and Reactors under

Dynamic Conditions for Energy Storage and Conversion" (Project no. 406474220, GL 290/12-2 and DE 659/13-2).

The authors thank Omegadot Software & Consulting GmbH, Limburgerhof, Germany, for the cost-free academic license of DETCHEM. The authors also thank M. Icker and M. Roßberg, both Leipzig University, for NMR and elemental analysis, respectively.

Open access funding enabled and organized by Projekt DEAL.

Conflicts of Interest

The authors declare no conflicts of interest.

Data Availability Statement

The data that support the findings of this study are available from the corresponding author upon reasonable request.

References

1. IPCC, Climate Change 2023: Synthesis Report Geneva 2023.

2. M. Erans, E. S. Sanz-Pérez, D. P. Hanak, Z. Clulow, D. M. Reiner, and G. A. Mutch, "Direct Air Capture: Process Technology, Techno-Economic and Socio-Political Challenges," *Energy & Environmental Science* 15 (2022): 1360–1405, https://doi.org/10.1039/D1EE03523A.

3. UNFCCC, The Paris Agreement Paris 2015.

4. D. W. Keith, G. Holmes, D. S. Angelo, and K. Heidel, "A Process for Capturing CO_2 From the Atmosphere," *Joule* 2 (2018): 1573–1594, https://doi.org/10.1016/j.joule.2018.05.006.

5. IEA, Direct Air Capture 2022 Paris 2022.

6. S. Baker, J. Stolaroff, G. Peridas, et al., Getting to Neutral: Options for Negative Carbon Emissions in California 2020, https://doi.org/10.2172/1597217.

7. N. McQueen, K. V. Gomes, C. McCormick, K. Blumanthal, M. Pisciotta, and J. Wilcox, "A Review of Direct Air Capture (DAC): Scaling up Commercial Technologies and Innovating for the Future," *Progress in Energy* 3 (2021): 032001, https://doi.org/10.1088/2516-1083/abf1ce.

8. A. Scott, "Sucking Carbon Dioxide From Air in Iceland," *Chemical & Engineering News* 102 (2024): 24–29, https://doi.org/10.1021/cen-10217-cover.

9. X. Wang and C. Song, "Carbon Capture From Flue Gas and the Atmosphere: A Perspective," *Frontiers in Energy Research* 8 (2020): 56084.

10. X. Yan, L. Zhang, Y. Zhang, G. Yang, and Z. Yan, "Amine-Modified SBA-15: Effect of Pore Structure on the Performance for CO 2 Capture," *Industrial & Engineering Chemistry Research* 50 (2011): 3220–3226, https://doi.org/10.1021/ie101240d.

11. G. Zhang, P. Zhao, L. Hao, and Y. Xu, "Amine-Modified SBA-15(P): A Promising Adsorbent for CO_2 Capture," *Journal of CO2 Utilization* 24 (2018): 22–33, https://doi.org/10.1016/j.jcou.2017.12.006.

12. X. Zhu, W. Xie, J. Wu, et al., "Recent Advances in Direct Air Capture by Adsorption," *Chemical Society Reviews* 51 (2022): 6574–6651, https://doi.org/10.1039/D1CS00970B.

13. D. S. Dao, H. Yamada, and K. Yogo, "Large-Pore Mesostructured Silica Impregnated With Blended Amines for CO 2 Capture," *Industrial & Engineering Chemistry Research* 52 (2013): 13810–13817, https://doi.org/10.1021/ie4020588.

14. K. Li, J. Jiang, S. Tian, F. Yan, and X. Chen, "Polyethyleneimine–Nano Silica Composites: A Low-Cost and Promising Adsorbent for CO_2 Capture," *Journal of Materials Chemistry A* 3 (2015): 2166–2175, https://doi.org/10.1039/C4TA04275A.

15. D. Panda, V. Kulkarni, and S. K. Singh, "Evaluation of Amine-based Solid Adsorbents for Direct Air Capture: A Critical Review," *Reaction Chemistry & Engineering* 8 (2022): 10–40, https://doi.org/10.1039/D2RE00211F.

16. J. C. Hicks, J. H. Drese, D. J. Fauth, M. L. Gray, G. Qi, and C. W. Jones, "Designing Adsorbents for CO_2 Capture From Flue Gas-Hyperbranched Aminosilicas Capable of Capturing CO_2 Reversibly," *Journal of the American Chemical Society* 130 (2008): 2902–2903, https://doi.org/10.1021/ja077795v.

17. H. Zhang, A. Goeppert, M. Czaun, G. K. S. Prakash, and G. A. Olah, "CO 2 Capture on Easily Regenerable Hybrid Adsorbents Based on Polyamines and Mesocellular Silica Foam. Effect of Pore Volume of the Support and Polyamine Molecular Weight," *RSC Advances* 4 (2014): 19403–19417, https://doi.org/10.1039/C4RA02145B.

18. A. A. Hosseini and M. J. Lashaki, "A Comprehensive Evaluation of Amine-Impregnated Silica Materials for Direct Air Capture of Carbon Dioxide," *Separation and Purification Technology* 325 (2023): 124580, https://doi.org/10.1016/j.seppur.2023.124580.

19. S. Azizian, "Kinetic Models of Sorption: A Theoretical Analysis," *Journal of Colloid and Interface Science* 276 (2004): 47–52, https://doi.org/10.1016/j.jcis.2004.03.048.

20. A. M. Alkadhem, M. A. Elgzoly, A. Alshami, and S. A. Onaizi, "Kinetics of CO_2 Capture by Novel Amine-Functionalized Magnesium Oxide Adsorbents," *Colloids and Surfaces A: Physicochemical and Engineering Aspects* 616 (2021): 126258, https://doi.org/10.1016/j.colsurfa.2021.126258.

21. R. Serna-Guerrero and A. Sayari, "Modeling Adsorption of CO_2 on Amine-Functionalized Mesoporous Silica. 2: Kinetics and Breakthrough Curves," *Chemical Engineering Journal* 161 (2010): 182–190, https://doi.org/10.1016/j.cej.2010.04.042.

22. A. G. Ritchie, "Alternative to the Elovich Equation for the Kinetics of Adsorption of Gases on Solids," *Journal of the Chemical Society, Faraday Transactions 1: Physical Chemistry in Condensed Phases* 73 (1977): 1650, https://doi.org/10.1039/f19777301650.

23. A. Heydari-Gorji and A. Sayari, "CO_2 capture on Polyethylenimine-Impregnated Hydrophobic Mesoporous Silica: Experimental and Kinetic Modeling," *Chemical Engineering Journal* 173 (2011): 72–79, https://doi.org/10.1016/j.cej.2011.07.038.

24. B. Guo, Y. Wang, X. Qiao, et al., "Experiment and Regeneration Kinetic Model Study on CO_2 Adsorbent Prepared From Fly Ash," *Chemical Engineering Journal* 421 (2021): 127865, https://doi.org/10.1016/j.cej.2020.127865.

25. X. Wang and C. Song, "Temperature-Programmed Desorption of CO_2 from Polyethylenimine-Loaded SBA-15 as Molecular Basket Sorbents," *Catalysis Today* 194 (2012): 44–52, https://doi.org/10.1016/j.cattod.2012.08.008.

26. X. Xu, C. Song, J. M. Andresen, B. G. Miller, and A. W. Scaroni, "Novel Polyethylenimine-Modified Mesoporous Molecular Sieve of MCM-41 Type as High-Capacity Adsorbent for CO 2 Capture," *Energy & Fuels* 16 (2002): 1463–1469, https://doi.org/10.1021/ef020058u.

27. X. Xu, C. Song, J. M. Andrésen, B. G. Miller, and A. W. Scaroni, "Preparation and Characterization of Novel CO_2 "Molecular Basket" Adsorbents Based on Polymer-Modified Mesoporous Molecular Sieve MCM-41," *Microporous and Mesoporous Materials* 62 (2003): 29–45, https://doi.org/10.1016/S1387-1811(03)00388-3.

28. J. Pazdera, D. Issayeva, J. Titus, R. Gläser, O. Deutschmann, and A. Jentys, "Impact of the Local Environment of Amines on the Activity for CO 2 Hydrogenation Over Bifunctional Basic—Metallic Catalysts," *ChemCatChem* 14 (2022): e202200620, https://doi.org/10.1002/cctc.202200620.

29. M. Robertson, J. Qian, and Z. Qiang, "Polymer Sorbent Design for the Direct Air Capture of CO_2," *ACS Applied Polymer Materials* 6 no. 23 (2023): 14169–14189, https://doi.org/10.1021/acsapm.3c03199.

30. A. Danon, P. C. Stair, and E. Weitz, "FTIR Study of CO_2 Adsorption on Amine-grafted SBA-15: Elucidation of Adsorbed Species," *The Journal of Physical Chemistry C* 115 (2011): 11540–11549, https://doi.org/10.1021/jp200914v.

31. W. C. Wilfong, C. S. Srikanth, and S. S. Chuang, "In Situ ATR and DRIFTS Studies of the Nature of Adsorbed CO_2 on Tetraethylenepen-

tamine Films," *ACS Applied Materials & Interfaces* 6 (2014): 13617–13626, https://doi.org/10.1021/am5031006.

32. Y. Zhai and S. S. Chuang, "The Nature of Adsorbed Carbon Dioxide on Immobilized Amines During Carbon Dioxide Capture From Air and Simulated Flue Gas," *Energy Technology* 5 (2017): 510–519, https://doi.org/10.1002/ente.201600685.

33. M. Wenzel, M. A. Zaheer, D. Issayeva, et al., "Flow MAS NMR for In Situ Monitoring of Carbon Dioxide Capture and Hydrogenation Using Nanoporous Solids," *The Journal of Physical Chemistry C* 125 (2021): 10219–10225, https://doi.org/10.1021/acs.jpcc.1c00037.

34. L. Mafra, T. Čendak, S. Schneider, et al., "Structure of Chemisorbed CO_2 Species in Amine-Functionalized Mesoporous Silicas Studied by Solid-State NMR and Computer Modeling," *Journal of the American Chemical Society* 139 (2017): 389–408, https://doi.org/10.1021/jacs.6b11081.

35. M. L. Pinto, L. Mafra, J. M. Guil, J. Pires, and J. Rocha, "Adsorption and Activation of CO_2 by Amine-Modified Nanoporous Materials Studied by Solid-State NMR and 13CO2 Adsorption," *Chemistry of Materials* 23 (2011): 1387–1395, https://doi.org/10.1021/cm1029563.

36. M. Ilkaeva, R. Vieira, J. M. Pereira, M. Sardo, I. Marin-Montesinos, and L. Mafra, "Assessing CO_2 Capture in Porous Sorbents via Solid-State NMR-Assisted Adsorption Techniques," *Journal of the American Chemical Society* 145 (2023): 8764–8769, https://doi.org/10.1021/jacs.3c00281.

37. A. H. Berge, S. M. Pugh, M. I. Short, et al., "Revealing Carbon Capture Chemistry with 17-Oxygen NMR Spectroscopy," *Nature Communications* 13 (2022): 1–11, https://doi.org/10.1038/s41467-022-35254-w.

38. P. V. Kortunov, M. Siskin, L. S. Baugh, and D. C. Calabro, "Situ Nuclear Magnetic Resonance Mechanistic Studies of Carbon Dioxide Reactions With Liquid Amines in Aqueous Systems: New Insights on Carbon Capture Reaction Pathways," *Energy & Fuels* 29 (2015): 5919–5939, https://doi.org/10.1021/acs.energyfuels.5b00850.

39. P. V. Kortunov, M. Siskin, L. S. Baugh, and D. C. Calabro, "Situ Nuclear Magnetic Resonance Mechanistic Studies of Carbon Dioxide Reactions With Liquid Amines in Non-Aqueous Systems: Evidence for the Formation of Carbamic Acids and Zwitterionic Species," *Energy & Fuels* 29 (2015): 5940–5966, https://doi.org/10.1021/acs.energyfuels.5b00985.

40. K. Basaran, U. Topcubasi, and T. Davran-Candan, "Theoretical Investigation of CO_2 Adsorption Mechanism Over Amine-Functionalized Mesoporous Silica," *Journal of CO2 Utilization* 47 (2021): 101492–101508, https://doi.org/10.1016/j.jcou.2021.101492.

41. B. Arstad, R. Blom, and O. Swang, "CO 2 Absorption in Aqueous Solutions of Alkanolamines: Mechanistic Insight From Quantum Chemical Calculations," *The Journal of Physical Chemistry A* 111 (2007): 1222–1228, https://doi.org/10.1021/jp065301v.

42. R. Afonso, M. Sardo, L. Mafra, and J. R. Gomes, "Unravelling the Structure of Chemisorbed CO_2 Species in Mesoporous Aminosilicas: A Critical Survey," *Environmental Science & Technology* 53 (2019): 2758–2767, https://doi.org/10.1021/acs.est.8b05978.

43. T. C. D. Santos, S. Bourrelly, P. L. Llewellyn, J. W. M. Carneiro, and C. M. Ronconi, "Adsorption of CO_2 on Amine-Functionalised MCM-41: Experimental and Theoretical Studies," *Physical Chemistry Chemical Physics* 17 (2015): 11095–11102, https://doi.org/10.1039/C5CP00581G.

44. X. Wang, V. Schwartz, J. C. Clark, et al., "Infrared Study of CO 2 Sorption Over "Molecular Basket" Sorbent Consisting of Polyethylenimine-Modified Mesoporous Molecular Sieve," *The Journal of Physical Chemistry C* 113 (2009): 7260–7268, https://doi.org/10.1021/jp809946y.

45. S. A. Didas, M. A. Sakwa-Novak, G. S. Foo, C. Sievers, and C. W. Jones, "Effect of Amine Surface Coverage on the Co-Adsorption of CO_2 and Water: Spectral Deconvolution of Adsorbed Species," *The Journal of Physical Chemistry Letters* 5 (2014): 4194–4200, https://doi.org/10.1021/jz502032c.

46. M. W. Hahn, J. Jelic, E. Berger, K. Reuter, A. Jentys, and J. A. Lercher, "Role of Amine Functionality for CO_2 Chemisorption on Silica," *The Journal of Physical Chemistry B* 120 (2016): 1988–1995, https://doi.org/10.1021/acs.jpcb.5b10012.

47. R. Ben Said, J. M. Kolle, K. Essalah, B. Tangour, and A. Sayari, "A Unified Approach to CO 2 –Amine Reaction Mechanisms," *ACS Omega* 5 (2020): 26125–26133, https://doi.org/10.1021/acsomega.0c03727.

48. Z. Chen, S. Deng, H. Wei, B. Wang, J. Huang, and G. Yu, "Polyethylenimine-Impregnated Resin for High CO_2 Adsorption: An Efficient Adsorbent for CO_2 Capture From Simulated Flue Gas and Ambient Air," *ACS Applied Materials & Interfaces* 5 (2013): 6937–6945, https://doi.org/10.1021/am400661b.

49. W. Wang, F. Liu, Q. zhang, G. Yu, and S. Deng, "Efficient Removal of CO_2 From Indoor Air Using a Polyethyleneimine-impregnated Resin and Its Low-Temperature Regeneration," *Chemical Engineering Journal* 399 (2020): 125734, https://doi.org/10.1016/j.cej.2020.125734.

50. Y. Miao, Z. He, X. Zhu, D. Izikowitz, and J. Li, "Operating Temperatures Affect Direct Air Capture of CO_2 in Polyamine-Loaded Mesoporous Silica," *Chemical Engineering Journal* 426 (2021): 131875, https://doi.org/10.1016/j.cej.2021.131875.

51. H. Zeng, X. Qu, D. Xu, and Y. Luo, "Porous Adsorption Materials for Carbon Dioxide Capture in Industrial Flue Gas," *Frontiers in Chemistry* 10 (2022): 939701, https://doi.org/10.3389/fchem.2022.939701.

52. Y. Kuwahara, D.-Y. Kang, J. R. Copeland, et al., "Enhanced CO 2 Adsorption Over Polymeric Amines Supported on Heteroatom-Incorporated SBA-15 Silica: Impact of Heteroatom Type and Loading on Sorbent Structure and Adsorption Performance," *Chemistry—A European Journal* 18 (2012): 16649–16664, https://doi.org/10.1002/chem.201203144.

53. S. Choi, M. L. Gray, and C. W. Jones, "Amine-Tethered Solid Adsorbents Coupling High Adsorption Capacity and Regenerability for CO 2 Capture From Ambient Air," *ChemSusChem* 4 (2011): 628–635, https://doi.org/10.1002/cssc.201000355.

54. A. Goeppert, H. Zhang, M. Czaun, et al., "Easily Regenerable Solid Adsorbents Based on Polyamines for Carbon Dioxide Capture From the Air," *ChemSusChem* 7 (2014): 1386–1397, https://doi.org/10.1002/cssc.201301114.

55. A. Goeppert, M. Czaun, R. B. May, G. K. S. Prakash, G. A. Olah, and S. R. Narayanan, "Carbon Dioxide Capture From the Air Using a Polyamine-Based Regenerable Solid Adsorbent," *Journal of the American Chemical Society* 133 (2011): 20164–20167, https://doi.org/10.1021/ja2100005.

56. G. Rim, F. Kong, M. Song, et al., "Sub-Ambient Temperature Direct Air Capture of CO_2 Using Amine-Impregnated MIL-101(Cr) Enables Ambient Temperature CO_2 Recovery," *JACS Au* 2 (2022): 380–393, https://doi.org/10.1021/jacsau.1c00414.

57. X. Yan, L. Zhang, Y. Zhang, K. Qiao, Z. Yan, and S. Komarneni, "Amine-Modified Mesocellular Silica Foams for CO_2 Capture," *Chemical Engineering Journal* 168 (2011): 918–924, https://doi.org/10.1016/j.cej.2011.01.066.

58. X. Feng, G. Hu, X. Hu, et al., "Tetraethylenepentamine-Modified Siliceous Mesocellular Foam (MCF) for CO 2 Capture," *Industrial & Engineering Chemistry Research* 52 (2013): 4221–4228, https://doi.org/10.1021/ie301946p.

59. M. Cao, C. Han, S. Wang, et al., "Investigation of Density, Viscosity and Derived Thermodynamic Properties of CO_2-Free and CO_2-Loaded Poly(ethylene Imine) Aqueous Systems at Different Temperatures and 0.1 MPa," *Journal of Molecular Liquids* 377 (2023): 121523, https://doi.org/10.1016/j.molliq.2023.121523.

60. W. Chaikittisilp, H.-J. Kim, and C. W. Jones, "Mesoporous Alumina-Supported Amines as Potential Steam-Stable Adsorbents for Capturing CO_2 From Simulated Flue Gas and Ambient Air," *Energy & Fuels* 25 (2011): 5528–5537, https://doi.org/10.1021/ef201224v.

61. F. Kong, G. Rim, M. Song, et al., "Research Needs Targeting Direct Air Capture of Carbon Dioxide: Material & Process Performance Characteristics under Realistic Environmental Conditions," *Korean Journal of Chemical Engineering* 39 (2022): 1–19, https://doi.org/10.1007/s11814-021-0976-0.

62. D. Wu, T. M. McDonald, Z. Quan, et al., "Thermodynamic Complexity of Carbon Capture in Alkylamine-functionalized Metal–Organic Frame-

works," *Journal of Materials Chemistry A* 3 (2015): 4248–4254, https://doi.org/10.1039/C4TA06496H.

63. R. Serna-Guerrero, E. Da'na, and A. Sayari, "New Insights Into the Interactions of CO 2 With Amine-Functionalized Silica," *Industrial & Engineering Chemistry Research* 47 (2008): 9406–9412, https://doi.org/10.1021/ie801186g.

64. C. Chen and S. Bhattacharjee, "Mesoporous Silica Impregnated With Organoamines for Post-Combustion CO 2 Capture: A Comparison of Introduced Amine Types," *Greenhouse Gases: Science and Technology* 7 (2017): 1116–1125, https://doi.org/10.1002/ghg.1720.

65. J. J. Lee, C.-H. Chen, D. Shimon, S. E. Hayes, C. Sievers, and C. W. Jones, "Effect of Humidity on the CO 2 Adsorption of Tertiary Amine Grafted SBA-15," *The Journal of Physical Chemistry C* 121 (2017): 23480–23487, https://doi.org/10.1021/acs.jpcc.7b07930.

66. T. S. Pierre and M. Geckle, "13- NMR Analysis of Branched Polyethyleneimine," *Journal of Macromolecular Science: Part A—Chemistry* 22 (1985): 877–887, https://doi.org/10.1080/00222338508056641.

67. D. R. Holycross and M. Chai, "Comprehensive NMR Studies of the Structures and Properties of PEI Polymers," *Macromolecules* 46 (2013): 6891–6897, https://doi.org/10.1021/ma4011796.

68. H. Jung, S. Jeon, D. H. Jo, J. Huh, and S. H. Kim, "Effect of Crosslinking on the CO_2 Adsorption of Polyethyleneimine-Impregnated Sorbents," *Chemical Engineering Journal* 307 (2017): 836–844, https://doi.org/10.1016/j.cej.2016.09.005.

69. A. V. Harpe, H. Petersen, Y. Li, and T. Kissel, "Characterization of Commercially Available and Synthesized Polyethylenimines for Gene Delivery," *Journal of Controlled Release* 69 (2000): 309–322, https://doi.org/10.1016/S0168-3659(00)00317-5.

70. H. Cai, F. Bao, J. Gao, T. Chen, S. Wang, and R. Ma, "Preparation and Characterization of Novel Carbon Dioxide Adsorbents Based on Polyethylenimine-Modified Halloysite Nanotubes," *Environmental technology* 36 (2015): 1273–1280, https://doi.org/10.1080/09593330.2014.984772.

71. J. N. Spencer, W. S. Wolbach, J. W. Hovick, L. Ansel, and K. J. Modarress, "Hydrogen Bonding by Alcohols and Amines," *Journal of Solution Chemistry* 14 (1985): 805–814, https://doi.org/10.1007/BF00646002.

72. Y. Meng, J. Jiang, A. Aihemaiti, et al., "Feasibility of CO_2 Capture From O2-Containing Flue Gas Using a Poly(ethylenimine)-Functionalized Sorbent: Oxidative Stability in Long-Term Operation," *ACS Applied Materials & Interfaces* 11 (2019): 33781–33791, https://doi.org/10.1021/acsami.9b08048.

73. H. V. Thakkar, A. J. Ruba, J. A. Matteson, M. P. Dugas, and R. P. Singh, "Accelerated Testing of PEI-Silica Sorbent Pellets for Direct Air Capture," *ACS Omega* 9 (2024): 45970–45982, https://doi.org/10.1021/acsomega.4c05639.

74. S. Bali, T. T. Chen, W. Chaikittisilp, and C. W. Jones, "Oxidative Stability of Amino Polymer–Alumina Hybrid Adsorbents for Carbon Dioxide Capture," *Energy & Fuels* 27 (2013): 1547–1554, https://doi.org/10.1021/ef4001067.

75. A. Heydari-Gorji and A. Sayari, "Thermal, Oxidative, and CO 2 -Induced Degradation of Supported Polyethylenimine Adsorbents," *Industrial & Engineering Chemistry Research* 51 (2012): 6887–6894, https://doi.org/10.1021/ie3003446.

76. P. Bollini, S. Choi, J. H. Drese, and C. W. Jones, "Oxidative Degradation of Aminosilica Adsorbents Relevant to Postcombustion CO 2 Capture," *Energy & Fuels* 25 (2011): 2416–2425, https://doi.org/10.1021/ef200140z.

77. A. Ahmadalinezhad and A. Sayari, "Oxidative Degradation of Silica-Supported Polyethylenimine for CO_2 Adsorption: Insights Into the Nature of Deactivated Species," *Physical Chemistry Chemical Physics* 16 (2014): 1529–1535, https://doi.org/10.1039/C3CP53928H.

78. W. C. Wilfong, B. W. Kail, C. W. Jones, C. Pacheco, and M. L. Gray, "Spectroscopic Investigation of the Mechanisms Responsible for the Superior Stability of Hybrid Class 1/Class 2 CO_2 Sorbents: A New Class 4 Category," *ACS applied materials & interfaces* 8 (2016): 12780–12791, https://doi.org/10.1021/acsami.6b02062.

79. Y. Zhai and S. S. C. Chuang, "Enhancing Degradation Resistance of Polyethylenimine for CO 2 Capture With Cross-Linked Poly(vinyl alcohol)," *Industrial & Engineering Chemistry Research* 56 (2017): 13766–13775, https://doi.org/10.1021/acs.iecr.7b03636.

80. M. M. Hantel, M. J. Armstrong, F. DaRosa, and R. l'Abee, "Characterization of Tortuosity in Polyetherimide Membranes Based on Gurley and Electrochemical Impedance Spectroscopy," *Journal of The Electrochemical Society* 164 (2017): A334–A339, https://doi.org/10.1149/2.1071702jes.

81. E. Andreoli, L. Cullum, and A. R. Barron, "Carbon Dioxide Absorption by Polyethylenimine-Functionalized Nanocarbons: A Kinetic Study," *Industrial & Engineering Chemistry Research* 54 (2015): 878–889, https://doi.org/10.1021/ie504277s.

82. X. Wang and C. Song, "Developing High-Capacity Solid "Molecular Basket" Sorbents for Selective CO 2 Capture and Separation," *Accounts of Chemical Research* 56 (2023): 3358–3368, https://doi.org/10.1021/acs.accounts.3c00444.

83. S. Brunauer, P. H. Emmett, and E. Teller, "Adsorption of Gases in Multimolecular Layers," *Journal of the American Chemical Society* 60 (1938): 309–319, https://doi.org/10.1021/ja01269a023.

84. E. P. Barrett, L. G. Joyner, and P. P. Halenda, "The Determination of Pore Volume and Area Distributions in Porous Substances. I. Computations From Nitrogen Isotherms," *Journal of the American Chemical Society* 73 (1951): 373–380, https://doi.org/10.1021/ja01145a126.

85. E. W. Washburn, "The Dynamics of Capillary Flow," *Physical Review* 17 (1921): 273–283, https://doi.org/10.1103/PhysRev.17.273.

86. A. Chatterjee and S. Schiewer, "Biosorption of Cadmium(II) Ions by Citrus Peels in a Packed Bed Column: Effect of Process Parameters and Comparison of Different Breakthrough Curve Models," *Clean: Soil, Air, Water* 39 (2011): 874–881, https://doi.org/10.1002/clen.201000482.

87. R. Chacko, K. Keller, S. Tischer, et al., "Automating the Optimization of Catalytic Reaction Mechanism Parameters Using Basin-Hopping: A Proof of Concept," *The Journal of Physical Chemistry C* 127 (2023): 7628–7639, https://doi.org/10.1021/acs.jpcc.2c08179.

88. D. E. Mears, "Tests for Transport Limitations in Experimental Catalytic Reactors," *Industrial & Engineering Chemistry Process Design and Development* 10 (1971): 541–547, https://doi.org/10.1021/i260040a020.

89. N. N. Avgul, A. V. Kiselev, and I. A. Lygina, "The Adsorption Energies of CO_2, SO2, (CH3)2CO and (C2H5)2O on Graphite," *Bulletin of the Academy of Sciences of the USSR Division of Chemical Science* 10 (1961): 1300–1307, https://doi.org/10.1007/BF00910098.

Supporting Information

Additional supporting information can be found online in the Supporting Information section.

Supporting File: cctc70531-sup-0001-SuppMat.docx.